



RESEARCH LETTER

10.1002/2014GL059738

Key Points:

- We estimate aerosol size distribution dependence on environment conditions
- Oceanic mesoscale variability affects aerosol size distribution
- We identified a distinct population of aerosols introduced through advection

Supporting Information:

- Readme
- Figure S1

Correspondence to:

I. Koren,
ilan.koren@weizmann.ac.il

Citation:

Lehahn, Y., I. Koren, Y. Rudich, K. D. Bidle, M. Trainic, J. M. Flores, S. Sharoni, and A. Vardi (2014), Decoupling atmospheric and oceanic factors affecting aerosol loading over a cluster of mesoscale North Atlantic eddies, *Geophys. Res. Lett.*, 41, doi:10.1002/2014GL059738.

Received 26 FEB 2014

Accepted 19 MAY 2014

Accepted article online 21 MAY 2014

Decoupling atmospheric and oceanic factors affecting aerosol loading over a cluster of mesoscale North Atlantic eddies

Yoav Lehahn¹, Ilan Koren¹, Yinon Rudich¹, Kay D. Bidle², Miri Trainic¹, Jorge Michel Flores¹, Shlomit Sharoni¹, and Assaf Vardi³

¹Department of Earth and Planetary Sciences, Weizmann Institute of Science, Rehovot, Israel, ²Institute of Marine and Coastal Sciences, Rutgers University, New Brunswick, New Jersey, USA, ³Department of Plant Sciences, Weizmann Institute of Science, Rehovot, Israel

Abstract Using shipboard and satellite measurements we explore the environmental factors affecting the number concentration of aerosols with diameter $100 < D < 1000$ nm over a cluster of three mesoscale (~ 10 – 100 km) eddies in the North Atlantic. Strongest sensitivity to environmental conditions was found in the $400 < D < 1000$ nm size range. In this size range particle concentrations were closely linked to the surface wind speed, indicating in situ production of sea spray aerosols by wind-driven processes. Particle concentrations were also affected by mesoscale variability in oceanic conditions at the vicinity of an anticyclonic eddy. In addition, a distinct aerosol population possibly produced at a distance of ~ 1000 – 2000 km from the study area was identified. The results highlight the importance of oceanic and atmospheric mesoscale processes in determining the characteristics of aerosols over the marine environment.

1. Introduction

Covering approximately 70% of the Earth's surface, the global ocean is one of the major sources of natural aerosols. Sea spray aerosols (SSA), which are emitted from the sea surface through wind-driven processes, contribute significantly to the Earth's radiative budget, through direct interaction with solar radiation [Bates *et al.*, 2006] or indirectly by affecting the microphysical properties of clouds [Andreae and Rosenfeld, 2008]. Yet the emissions and atmospheric burden of SSA are still poorly constrained, and estimates of their size-dependent production flux vary by an order of magnitude [de Leeuw *et al.*, 2011], largely due to the complexity of the SSA production process. While primarily dependent on the surface wind speed (W), SSA emission and properties may also depend on a large variety of oceanic and atmospheric factors, including atmospheric stability, relative humidity, sea surface temperature (SST), sea surface salinity (SSS), and the presence of surface-active materials [Lewis and Schwartz, 2004]. An improved quantitative understanding of SSA response to changes in environmental conditions is essential for accurate representation of their role in the climate system.

Here we explore the link between aerosol number concentration and changes in environmental conditions over a $2^\circ \times 2^\circ$ region in the North Atlantic Ocean. To untangle the contributions of different oceanic and atmospheric factors, we analyze variations over an area characterized by oceanic mesoscale (~ 10 – 100 km) variability in physical and biogeochemical parameters. Such variability patterns result from dynamical processes as horizontal stirring and vertical upwelling at the vicinity of mesoscale coherent eddies [Lévy *et al.*, 2012]. As recently shown, mesoscale eddies also have significant impact on atmospheric variables such as wind, clouds, and rainfall [Frenger *et al.*, 2013].

2. Data and Methods

2.1. In Situ Measurements

In situ data was collected aboard the R/V *Knorr* as part of the “North Atlantic Virus Infection of Coccolithophore Expedition” (NAVICE; KN207-03; <http://www.bco-dmo.org/dataset-deployment/455468>). Aerosol size distributions were measured using an optical particle counter (TSI model 3340, TSI Inc., Shoreview, MN, USA). Measurements represent light-scattering equivalent sizes of NIST traceable Polystyrene Latex Spheres. Air was constantly pumped through a PM₁₀ inlet heads from a 15 m ship mast. The air was

pulled through stainless steel conductive tubes, minimizing adsorption of particles onto the tube walls. Relative humidity in the inlets was reduced to 20–40% relative humidity (RH), using silica gel column dryers.

Measurements of SST, SSS, and chlorophyll fluorescence were performed by continuously sampling seawater from the ship's clean seawater inlet at the bow of the ship, nominally 5 m below the sea surface. Surface wind speed, relative humidity (RH), air temperature (T), and barometric pressure (P) measurements were taken at the bow mast at a height of 15.5 m above the waterline. Oceanic and meteorological data were sampled in 60 s intervals.

2.2. Satellite Retrieval of Oceanic Variables

Regional surface concentrations of surface chlorophyll (Chl) and particulate inorganic carbon (PIC) were derived from the Moderate Resolution Imaging Spectroradiometer (MODIS) aboard Aqua. The data set was comprised of 4 km L3 images obtained from the ocean color data distribution site (<http://oceandata.sci.gsfc.nasa.gov/>).

Geostrophic velocity field was obtained from the Archiving, Validation, and Interpretation of Satellite Oceanographic data database (<http://www-aviso.cnes.fr>). The data are gridded on a $1/3^\circ \times 1/3^\circ$ Mercator grid, with one data file every 7 days. Lagrangian coherent structures (LCS) [Haller and Yuan, 2000] were derived from calculation of finite-size Lyapunov exponents. The cores of mesoscale eddies were characterized from maps of the Okubo-Weiss parameter (OW) [Okubo, 1970; Weiss, 1991], which is a measure of the relative dominance of vorticity (associated with the eddy's core, negative OW) and deformation (associated with the eddy's periphery, positive OW).

2.3. Air Mass Trajectories and Associated Wind Speed

Hourly back trajectories over 48 h were calculated with the Air Resources Laboratory's Hybrid Single-Particle Lagrangian Integrated Trajectory model, using the Real-time Environmental Applications and Display System [Draxler and Rolph, 2014; Rolph, 2014]. Terminal height was set to 20, 50, 100, and 500 m. Results vary little for the different heights. To facilitate the presentation of the results only trajectories terminated at 20 m are shown.

Surface wind speeds along the air mass trajectories were derived from the Special Sensor Microwave Imager (SSM/I) aboard the Defense Meteorological Satellite Program satellite F17 and from WindSat aboard the satellite Coriolis. For both sensors, the spatial resolution is 25 km with two samples per day. WindSat data are produced by Remote Sensing Systems (RSS) and sponsored by the NASA Earth Science MEaSUREs DISCOVER Project and the NASA Earth Science Physical Oceanography Program. SSM/I data are produced by RSS and sponsored by the NASA Earth Science MEaSUREs Program. RSS data are available at www.remss.com. Daily wind speeds along the air mass trajectories were derived by averaging all available observations at a given day over a $2^\circ \times 2^\circ$ region centered at the air mass location 24 and 48 h prior to the trajectory initiation.

3. Results and Discussion

Aerosol sampling was performed in a system of two anticyclonic and one cyclonic mesoscale eddies (Figure 1a) during an 11 d period (1–11 July 2012). The three eddies were encircled by LCS (Figure 1b), indicating that they were fairly isolated and subject to little mixing with their surroundings [Lehahn et al., 2011]. The two anticyclonic eddies were also characterized by high PIC signature (Figure 1c), associated with CaCO_3 plates (coccoliths) that cover coccolithophore cells. High corresponding in situ coccolith abundance and backscatter was documented in the upper mixed layer of "Eddy A" (Figure 1a) (Y. Lehahn et al., Decoupling physical and biological processes to assess the impact of viruses on algal blooms from satellite data, in preparation), thereby confirming this satellite PIC signature.

3.1. Dependence on Surface Wind Speed

In general, the measured aerosol size distribution between 100 and 1000 nm was similar to previous observations in clean maritime conditions (Figure 2a) [O'Dowd et al., 2001]. It was characterized by two peaks, the first centered at around 200 nm and the second centered at around 500 nm. While the 200 nm peak varies little in time and space, the 500 nm peak and the associated concentrations (C) of particles in the 400–1000 nm range varied in response to changes in environmental conditions, most prominently surface wind speeds (W). For wind speeds higher than 4 m s^{-1} , which are commonly considered as the

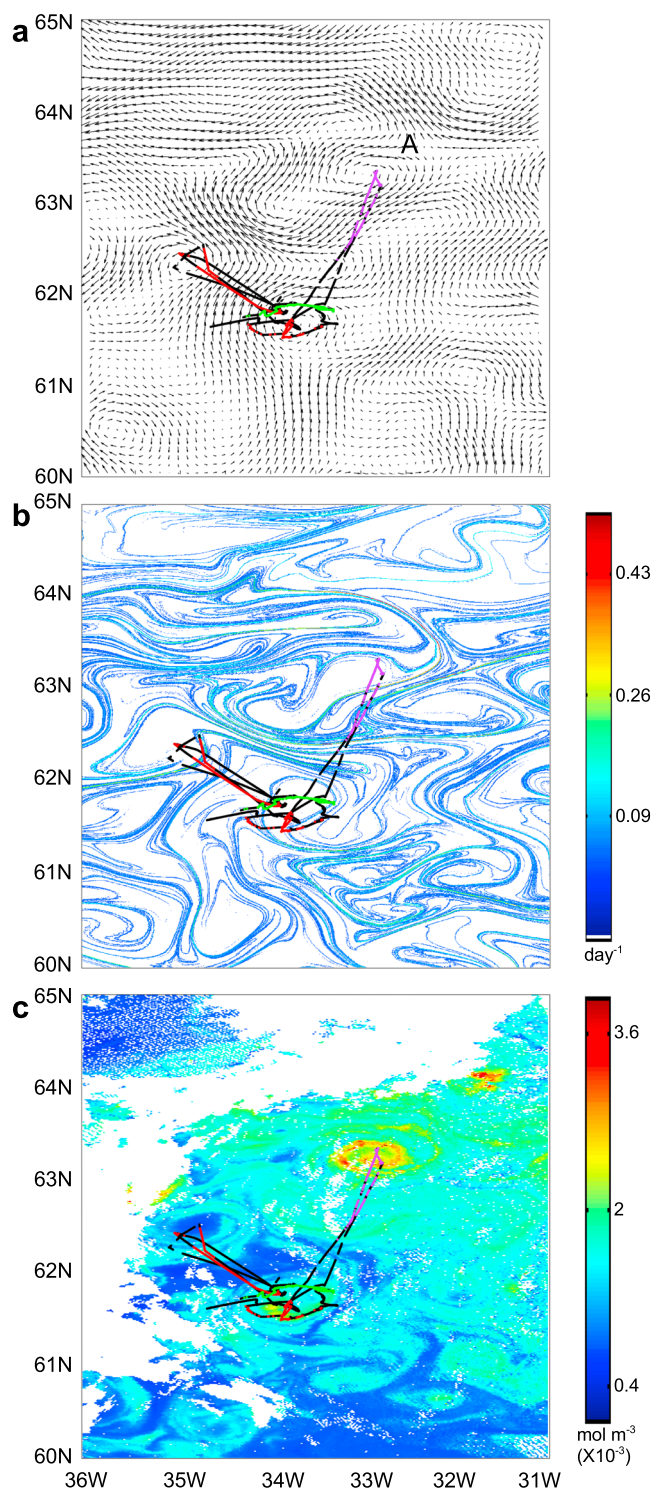


Figure 1. Satellite-derived (a) geostrophic surface currents, (b) Lagrangian coherent structures (LCS), and (c) particulate inorganic carbon (PIC). Solid lines mark sections of the 11 days ship track: red and green sections mark the locations associated with sampling of the LWLA and LWHA aerosol populations, respectively. Purple section marks the 24 h leg used for quantifying the impact of mesoscale changes in oceanic variability, at the vicinity of the anticyclonic eddy marked by the letter A (see text).

threshold value for whitecap formation [O'Dowd and de Leeuw, 2007], concentrations of 400–1000 nm particles significantly correlate ($R = 0.68$, $P < 0.01$) with W (Figure 2b). The dependence of aerosol concentrations on W is indicative of local wind-driven SSA production, with wind speed of between 4 and 5 m s⁻¹ being the threshold value for triggering the emission process [Lehahn et al., 2010].

3.2. Low-Wind Aerosol Populations

When focusing on the low wind ($W < 4$ m s⁻¹) regime, the dependence on surface wind speed (Figure 2b), reveals two distinct populations: (i) a low-concentration population (denoted LWLA, Figure 2b) that is linked to the main cluster, thereby showing an expected dependence on surface wind; and (ii) a high-concentration population (denoted LWHA, Figure 2b) that is clearly identified as a distinct cluster separated from the general relationship with W . These two populations fundamentally differ in their size distribution. The LWLA population follows a similar size distribution pattern as those measured in other wind regimes, with lowest concentrations at the range 400–1000 nm (Figure 2a, solid red line). The LWHA population has a different size distribution (with respect to the other wind regimes), with lower concentrations in the $200 < D < 300$ nm range, and relatively high concentrations in the $400 < D < 1000$ nm range (Figure 2a, red dashed line).

The two low-wind aerosol populations were also distinguished in time and associated meteorological conditions. The LWLA population was found intermittently over a 6 day period between 4 and 9 July and is associated with a high-pressure system (measured surface pressure of 1023 ± 1.6 mb). The LWHA population appeared during a ~48 h event between 1 and 3 July and

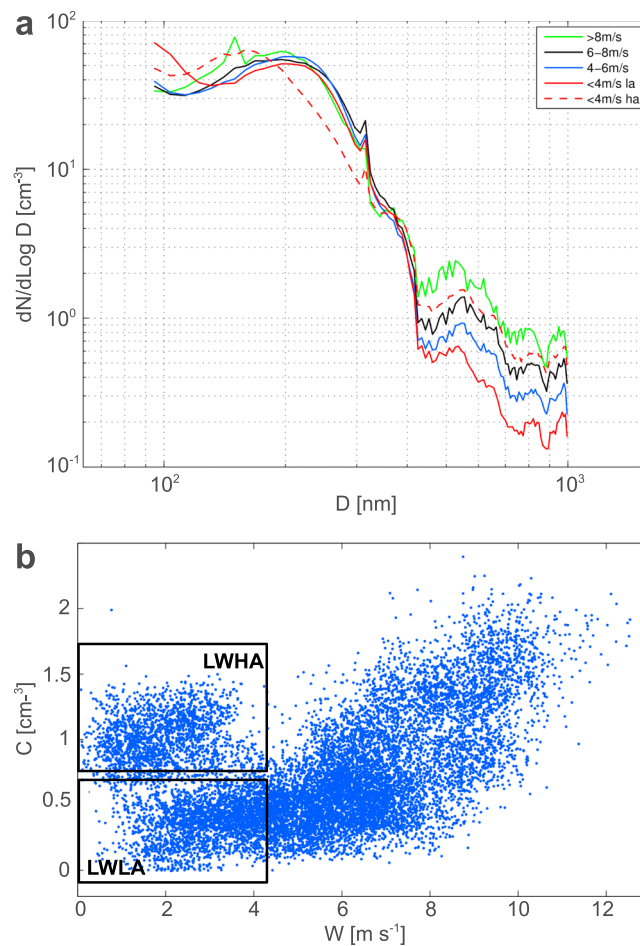


Figure 2. (a) Aerosol number size distribution throughout the 11 days period for different wind regimes. Solid and dashed red lines are associated with the low-wind ($W < 4$ m/s) aerosol populations LWLA and LWHA, respectively. (b) Concentrations of $400 < D < 1000$ nm aerosols plotted against surface wind speed. Lower and upper boxes delineate the clusters associated with the LWLA and LWHA aerosol populations, respectively.

and associated air mass and wind history, the LWHA population probably corresponds to SSA that were produced by relatively strong winds of up to 9.5 m s^{-1} , 24–48 h prior to sampling. Accordingly, the particles were transported ~ 1000 – 2000 km before settling at a low-wind area, at which time they were sampled. The characterization of a distinct population that is associated with transport of SSA from a remote location emphasizes the important role of atmospheric mesoscale (~ 10 – 1000 km) variability in modulating properties of marine boundary layer aerosols, supporting previous observations by Anderson *et al.* [2003]. Identification of a distinct transported SSA population was made possible due to a unique combination of low wind speeds at the sampling location (average W on 2 July, when almost all aerosols were characterized as LWHA, was $1.5 \pm 0.7 \text{ m s}^{-1}$) and strong winds along the air mass trajectory prior to the sampling time. It is likely to assume that sampling during other periods also included contribution of transported aerosols, which may have masked part of the signature of the locally produced SSA. Estimates of W along the air mass trajectories suggest that in addition to 2 July, transported SSA may be found substantially in 7, 10, and 11 July (averaged W along the 48 h air mass trajectories initiate at 12:00 were $6.6 \pm 2.9 \text{ m s}^{-1}$, $8.2 \pm 0.3 \text{ m s}^{-1}$, and $7.1 \pm 2.8 \text{ m s}^{-1}$, respectively; Figure S1 in the supporting information). Nevertheless, the relatively strong winds measured in situ during those days (averaged values of $6.4 \pm 0.9 \text{ m s}^{-1}$, $7.6 \pm 1.7 \text{ m s}^{-1}$, and $9.3 \pm 1 \text{ m s}^{-1}$ during 7, 10, and 11 July, respectively) indicate to a strong signature of locally produced SSA, in addition to the possible effect of transported aerosols. During the rest of the sampling period, we estimate the contribution of

was associated with a low-pressure system (measured surface pressure of 1013 ± 2.8 mb).

The origin of the two populations was investigated by analysis of the air mass history and of the surface winds associated with it, 48 h prior to the sampling of the two populations (Figure 3). Backward air mass trajectories were initiated on 2 July (for the LWHA population) and 4 July (for the LWLA population), when highest numbers of samples were classified as LWHA and LWLA, respectively. The trajectories were initiated at 12:00. During the 48 h prior to the sampling, the LWLA air mass traveled a relatively short distance in the vicinity of the sampling area (Figure 3a, red line) and was associated with moderate winds (averaged W along the 48 h trajectory was $4.3 \pm 1.08 \text{ m s}^{-1}$, Figure 3b). The LWHA air mass followed a longer trajectory (Figure 3a, black line) and was associated with relatively strong winds (averaged surface wind speed along the trajectory was $7.7 \pm 2.4 \text{ m s}^{-1}$, Figure 3c).

The relatively low aerosol concentrations, together with the overall agreement with the different wind regimes, suggest that the LWLA population represents the regional background aerosol field. In contrast, given their much higher concentration

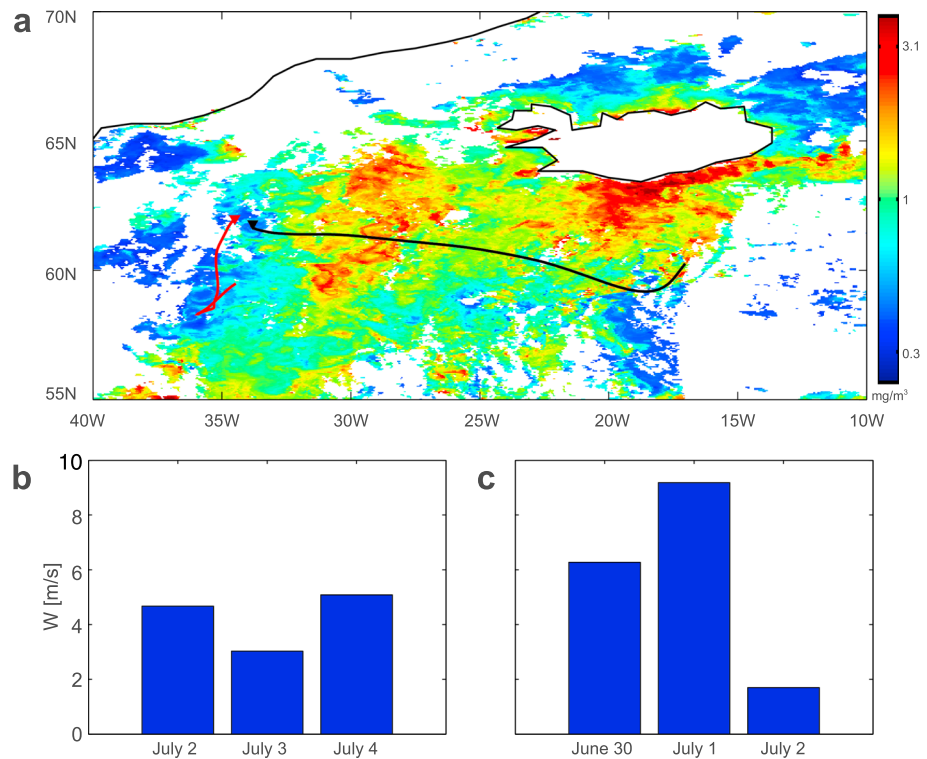


Figure 3. (a) Forty-eight hours back trajectory of air mass associated with the LWLA (initiated on 4 July at 12:00, red line) and LWHA (initiated on 2 July at 12:00, black line) aerosol populations. Triangles mark the corresponding sampling locations at 34.5°W/62°N and 33.8°W/61.8°N. The trajectories are superimposed on MODIS-Aqua surface chlorophyll image for the period 29 June to 6 July 2012. (b, c) Daily averages of satellite-derived surface wind speeds along the LWLA and LWHA air mass trajectories, respectively.

transported SSA to be small, due to low winds ($\sim 5 \text{ m s}^{-1}$ or smaller) along the 48 h backward air mass trajectories (Figure S1).

3.3. Dependence on Mesoscale Oceanic Variability

To investigate the possible impact of oceanic variability, and to untangle it from the dominant effect of surface wind speed, we focus on a leg from 6 July that was characterized by relatively constant atmospheric conditions and varying oceanic conditions (purple section of the ship's track in Figure 1). The leg took place at the vicinity of an anticyclonic eddy (denoted A in Figure 1). Surface winds were relatively strong and homogeneous ($7.7 \pm 0.9 \text{ m s}^{-1}$). To further reduce the variability associated with wind speed, we restrict the analysis to samples corresponding to $W > 8 \text{ m s}^{-1}$, resulting in average surface winds of $8.6 \pm 0.5 \text{ m s}^{-1}$. In both cases average concentrations of $400 < D < 1000 \text{ nm}$ aerosols were $1.0 \pm 0.3 \text{ cm}^{-3}$. Surface wind speeds along 48 h backward air mass trajectories prior to the sampling time were relatively low (average W along three trajectories initiated at the sampling location on 6 July at 6:00, 12:00, and 18:00 was $5.1 \pm 0.6 \text{ m s}^{-1}$), suggesting relatively small contribution of transported SSA. In agreement with the low atmospheric variability, during the leg there was little correlation between concentrations of $400 < D < 1000 \text{ nm}$ aerosols and atmospheric variables (Figure 4, green bars). In contrast, aerosol concentrations during the leg were strongly linked to a number of oceanic variables (Figure 4, blue bars).

The correlation with the OW parameter, which is a measure to morphology of mesoscale eddies as observed in a satellite-derived velocity field [Lehahn et al., 2011], indicates that aerosol concentrations varied in space in response to mesoscale oceanic variability at the vicinity of eddy A. This is supported by the fact the leg included crossing of LCS (Figure 1b), which may separate between water bodies with distinct physical and biogeochemical characteristics [Lehahn et al., 2007; d'Ovidio et al., 2010; Efrati et al., 2013].

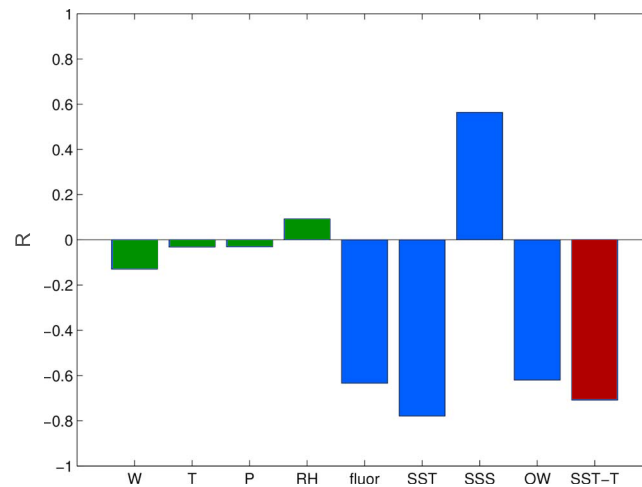


Figure 4. Correlation coefficients between concentration of aerosols in the $400 < D < 1000$ nm size range and different environmental variables, throughout a 24 h leg at the vicinity of eddy A (Figure 1, purple section). Number of samples is 536. Green and blue bars correspond to atmospheric and oceanic variables, respectively. Maroon bar corresponds to the temperature difference between the water and the atmosphere (SST-T). W – surface wind speed; T – air temperature; P – air pressure; RH – relative humidity; fluor – chlorophyll fluorescence; SST – sea surface temperature; SSS – sea surface salinity; OW – Okubo-Weiss parameter.

Since the different oceanic variables are coupled and vary simultaneously with the transition between water masses, it is difficult to attribute the spatial change in $400 < D < 1000$ aerosol concentrations to a single variable. Furthermore, because of the complexity of the SSA production mechanism, changes in a given parameter may have different, and possibly contrasted, results under different environmental conditions. For example, laboratory experiments [Mårtensson *et al.*, 2003; Hultin *et al.*, 2011] and global observational studies [Jaeglé *et al.*, 2011] report on both positive and negative correlations between SSA production and SST. Similarly, contradictory results were reported on possible link between atmospheric stability, which is associated to the difference between air temperature and SST (Figure 4, maroon bar), and the coverage and persistence of whitecaps [Lewis and Schwartz, 2004].

The spatial scale of the observed variability (oceanic mesoscale; ~ 10 – 100 km), which dominates the planktonic ecosystem [d'Ovidio *et al.*, 2010], implies that the change in aerosol properties during the leg was associated with changes in biogenic composition of the surface waters [O'Dowd *et al.*, 2004; Fuentes *et al.*, 2010]. Specifically, the change in $400 < D < 1000$ aerosol concentrations is suggested to be associated with surfactants, which were shown to affect the primary production of submicron marine aerosols [Sellegri *et al.*, 2006]. Furthermore, the negative correlation with chlorophyll fluorescence (Figure 4) is in agreement with Sellegri *et al.* [2006] laboratory experiments that show a decrease in the amplitude of mode 3 (300 nm) of the aerosols size distribution in response to surfactant addition. Alternatively, the negative correlation can correspond to changes in surface concentrations of small organic particulates and dissolved organic matter released during phytoplankton predation and viral lysis [Quinn and Bates, 2011].

Acknowledgments

We thank the captain and crew of the R/V *Knorr* and the Marine Facilities and Operations personnel at the Woods Hole Oceanographic Institution for their assistance during the NAVICE cruise. This project was supported by NSF grant OCE-1061883 to K.D.B. and A.V. A.V. and S.S. are supported by a European Research Council (ERC) StG (INFOTROPIC grant 280991) and the generous support of Edith and Nathan Goldenberg Career Development Chair to A.V. I.K., Y.L., and M.T. are supported by the European Research Council under the European Union's Seventh Framework Programme (FP7/2007-2013)/ERC (CAPRI, grant 306965). J.M.F. is supported by a research grant from the Jinich Postdoctoral Fellowship.

The Editor thanks one anonymous reviewer for his/her assistance in evaluating this paper.

4. Summary and Conclusions

Using continuous shipboard aerosol size distribution measurements, in conjunction with measurements of oceanic and atmospheric variables, we investigate the environmental factors that affect the number concentration of submicron particles over a cluster of mesoscale eddies in the North Atlantic. The strongest variability was observed in the $400 < D < 1000$ nm size range, where particle concentrations were closely linked to surface wind speed and to mesoscale changes in oceanic conditions in the vicinity of an anticyclonic mesoscale eddy. Considering the importance of mesoscale dynamics in shaping the physical and biogeochemical oceanic landscape, further investigation of variability patterns at this scale will improve our ability to correctly interpret and represent the role of oceanic processes in regulating marine aerosol production. Furthermore, the presence of a distinct aerosol population associated with advection from a distance of ~ 1000 – 2000 km highlights the importance of atmospheric mesoscale processes in structuring the distribution of marine boundary layer aerosols.

References

- Anderson, T., R. Charlson, D. Winker, J. Ogren, and K. Holmen (2003), Mesoscale variations of tropospheric aerosols, *J. Atmos. Sci.*, *60*, 119–136.
- Andreae, M. O., and D. Rosenfeld (2008), Aerosol-cloud-precipitation interactions. Part 1. The nature and sources of cloud-active aerosols, *Earth Sci. Rev.*, *89*, 13–41.
- Bates, T. A., et al. (2006), Aerosol direct radiative effects over the northwest Atlantic, northwest Pacific, and North Indian Oceans: Estimates based on in-situ chemical and optical measurements and chemical transport modeling, *Atmos. Chem. Phys.*, *6*, 1657–1732.

- de Leeuw, G., E. L. Andreas, M. D. Anguelova, C. W. Fairall, E. R. Lewis, C. O'Dowd, M. Schulz, and S. E. Schwartz (2011), Production flux of sea spray aerosol, *Rev. Geophys.*, *49*, RG2001, doi:10.1029/2010RG000349.
- d'Ovidio, F., S. De Monte, S. Alvain, Y. Dandonneau, and M. Lévy (2010), Fluid dynamical niches of phytoplankton types, *Proc. Natl. Acad. Sci. U. S. A.*, *107*, 18,366–18,370.
- Draxler, R. R., and G. D. Rolph (2014), HYSPLIT (Hybrid Single-Particle Lagrangian Integrated Trajectory) Model access via NOAA ARL READY Website, NOAA Air Resources Laboratory, Silver Spring, Md. [Available at <http://ready.arl.noaa.gov/HYSPLIT.php>.]
- Efrati, S., Y. Lehahn, E. Rahav, N. Kress, B. Herut, I. Gertman, R. Goldman, T. Ozer, M. Lazar, and E. Heifetz (2013), Intrusion of coastal waters into the pelagic Eastern Mediterranean: In situ and satellite-based characterization, *Biogeosciences*, *10*, 3349–3357, doi:10.5194/bg-10-3349-2013.
- Frenger, I., N. Gruber, R. Knutti, and M. Münnich (2013), Imprint of Southern Ocean eddies on winds, clouds and rainfall, *Nat. Geosci.*, *6*, 698–712, doi:10.1038/ngeo1863.
- Fuentes, E., H. Coe, D. Green, G. de Leeuw, and G. McFiggans (2010), On the impacts of phytoplankton-derived organic matter on the properties of the primary marine aerosol—Part 1: Source fluxes, *Atmos. Chem. Phys.*, *11*, 9295–9317, doi:10.5194/acp-10-9295-2010.
- Haller, G., and G. Yuan (2000), Lagrangian coherent structures and mixing in two-dimensional turbulence, *Physica D*, *147*, 352–370, doi:10.1016/S0167-2789(00)00142-1.
- Hultin, K. A. H., R. Krejci, J. Pinhassi, L. Gomez-Consarnau, E. M. Mårtensson, Å. Hagström, and E. D. Nilsson (2011), Aerosol and bacterial emissions from Baltic seawater, *Atmos. Res.*, *99*, 1–14.
- Jaeglé, L., P. K. Quinn, T. S. Bates, B. Alexander, and J.-T. Lin (2011), Global distribution of sea salt aerosols: New constraints from in situ and remote sensing observations, *Atmos. Chem. Phys.*, *11*, 3137–3157, doi:10.5194/acp-11-3137-2011.
- Lehahn, Y., F. d'Ovidio, M. Lévy, and E. Heifetz (2007), Stirring of the northeast Atlantic spring bloom: A Lagrangian analysis based on multi-satellite data, *J. Geophys. Res.*, *112*, C08005, doi:10.1029/2006JC003927.
- Lehahn, Y., I. Koren, E. Boss, Y. Ben-Ami, and O. Altaratz (2010), Estimating the maritime component of aerosol optical depth and its dependency on surface wind speed using satellite data, *Atmos. Chem. Phys.*, *10*, 6711–6720, doi:10.5194/acp-10-6711-2010.
- Lehahn, Y., F. d'Ovidio, M. Lévy, Y. Amitai, and E. Heifetz (2011), Long range transport of a quasi isolated chlorophyll patch by an Agulhas ring, *Geophys. Res. Lett.*, *38*, L17201, doi:10.1029/2011GL048502.
- Lévy, M., R. Ferrari, P. J. P. Franks, A. P. Martin, and P. Rivière (2012), Bringing physics to life at the submesoscale, *Geophys. Res. Lett.*, *39*, L14602, doi:10.1029/2012GL052756.
- Lewis, E., and S. Schwartz (2004), *Sea Salt Aerosols Production: Mechanisms, Methods, Measurements and Models: A Critical Review*, AGU, Washington, D. C.
- Mårtensson, E. M., E. D. Nilsson, G. de Leeuw, L. H. Cohen, and H.-C. Hansson (2003), Laboratory simulations and parameterization of the primary marine aerosol production, *J. Geophys. Res.*, *108*(D9), 4297, doi:10.1029/2002JD002263.
- O'Dowd, C. D., E. Becker, and M. Kulmala (2001), Mid-latitude North-Atlantic aerosol characteristics in clean and polluted air, *Atmos. Res.*, *58*, 167–185.
- O'Dowd, C., and G. de Leeuw (2007), Marine aerosol production: A review of the current knowledge, *Philos. Trans. R. Soc., A*, *365*, 1753–1774, doi:10.1098/rsta.2007.2043.
- O'Dowd, C., M. C. Facchini, F. Cavalli, D. Ceburnis, M. Mircea, S. Decesari, S. Fuzzi, Y. J. Yoon, and J.-P. Putaud (2004), Biogenically driven organic contribution to marine aerosol, *Nature*, *431*, 676–680.
- Okubo, A. (1970), Horizontal dispersion of floatable particles in the vicinity of velocity singularities such as convergences, *Deep Sea Res.*, *17*, 445–454.
- Quinn, P. K., and T. S. Bates (2011), The case against climate regulation via oceanic phytoplankton sulphur emissions, *Nature*, *480*, doi:10.1038/nature10580.
- Rolph, G. D. (2014), Real-time Environmental Applications and Display System (READY) Website, NOAA Air Resources Laboratory, Silver Spring, Md. [Available at <http://ready.arl.noaa.gov>.]
- Sellegrì, K., C. D. O'Dowd, Y. J. Yoon, S. G. Jennings, and G. de Leeuw (2006), Surfactants and submicron sea spray generation, *J. Geophys. Res.*, *111*, D22215, doi:10.1029/2005JD006658.
- Weiss, J. (1991), The dynamics of enstrophy transfer in two-dimensional hydrodynamics, *Physica D*, *48*, 273–294.